J. Iron Steel Res. Int. (2021) 28:1541–1550
https://doi.org/10.1007/s42243-021-00683-2

ORIGINAL PAPER

Effect of CaF_2 and CaO/Al_2O_3 on viscosity and structure of TiO_2-bearing slag for electroslag remelting

Jian-tao Ju[1,2] · Kang-shuai Yang[1] · Zhi-hong Zhu[1] · Yue Gu[1] · Li-zhong Chang[3]

Received: 10 May 2021 / Revised: 17 July 2021 / Accepted: 5 August 2021 / Published online: 12 November 2021

Abstract
The relationship between the viscosity and structure of CaF_2–CaO–Al_2O_3–MgO–TiO_2 slag with different CaF_2 contents and CaO/Al_2O_3 ratios was studied using the rotating cylinder method, Fourier transform infrared spectroscopy, and Raman spectrometry. The activity coefficients of CaF_2 and the CaO/Al_2O_3 ratio were determined to understand the correlation between viscosity and structure of the slag. The results suggest that the slag viscosity reduces gradually with an increase in CaF_2 content from 14.1 to 28.1 wt.% or CaO/Al_2O_3 ratio from 0.9 to 1.5, and correspondingly apparent activation energy for viscous flow reductions. The addition of CaF_2 does not change the structure of the molten slag; however, the relaxation effect of the anionic species and the hindrance effect of the cationic species are promoted by substituting part of the non-bridging oxygens (NBO) with F^- ions from CaF_2, which is attributed to the formation of NBO–Ca^{2+}–F^- and NBO–Ca^{2+}–NBO, respectively. However, as the CaO/Al_2O_3 ratio increases, some of the Q^4 units in the aluminate structure are depolymerized into Q^2 units, so that the relative strength of the Al–O–Al linkage decreases, and the relative fraction of $Ti_2O_6^{4-}$ chains increases, whereas that of O–Ti–O chains decreases slightly, resulting in depolymerization on the slag structure. Additionally, the effect of the CaO/Al_2O_3 ratio on the structure was greater than that of CaF_2 because of the greater depolymerization effect. The variation in the activity can indirectly explain the relationship between the viscosity and structure of the aluminate structural units based on thermodynamic analysis.

Keywords Viscosity · TiO_2-bearing slag · Fourier transform infrared spectroscopy · Raman spectrum · Thermodynamic

1 Introduction

Electroslag remelting (ESR) is a general production process for high-quality steel and alloys [1]. To achieve an excellent quality ingot during the remelting process, it is important to study the design of the slag composition and its physicochemical properties because the slag significantly affects the quality of the ingot, such as inclusions and desulfurization [2]. In the ESR process, the viscosity of molten slag has three main effects: (1) the surface quality of the ingot by forming a slag film [3]; (2) the velocity of molten steel droplets and molten slag–steel reaction time [4, 5]; and (3) the removal of nonmetallic inclusions and dense extent of solidified metal. Presently, the high-fluorine slag is widely applied because CaF_2 has the characteristics of significantly lowering the viscosity and liquidus temperature of the slag, but it has severe problems with harmful and volatile fluorides, environmental pollution, and chemical constituent changes, resulting in a prominent viscosity variation in the ESR slag [6, 7]. Thus, studies on the relatively low-fluorine slag in ESR slag have attracted interest.

The addition of CaF_2 reduced the viscosity of the molten slag. According to a study by Lao et al. [8], CaF_2 existed in the slag in the form of Ca–F bonds in the range of 40–80 wt.% and had no effect on the structure. However, Park et al. [9] found that for CaF_2 contents within the range of 5–15 wt.%, its effect on viscosity could be explained as a reduction in the degree of polymerization through F^- and

✉ Jian-tao Ju
jujiantao_0033@163.com

[1] School of Metallurgical Engineering, Xi'an University of Architecture and Technology, Xi'an 710055, Shaanxi, China

[2] Shaanxi Engineering Research Center of Metallurgical, Xi'an 710055, Shaanxi, China

[3] School of Metallurgy Engineering, Anhui University of Technology, Ma'anshan 243002, Anhui, China

O^{2-} ions. The effect of CaF_2 concentration on the slag structure based on the above analysis is controversial. Additionally, the effect of CaO and Al_2O_3 contents in the slag on the viscosity is quite important. The CaO/Al_2O_3 (C/A) ratio of conventional ESR slag is approximately unity to reach a relatively lower liquidus temperature based on ternary phase diagrams of the CaF_2–CaO–Al_2O_3 slag system [10]. However, the C/A ratio tends to increase as the smelting operation progresses, compared with that of slag before pre-melting, which is due to the chemical reaction of CaF_2 and Al_2O_3 [11]. Moreover, the addition of a few other oxides such as TiO_2, SiO_2 and MgO leads to pronounced diversification of the C/A ratio, causing significant changes in slag composition and viscosity [12]. Several studies have reported the effect of the C/A ratio on the viscosity. Yan et al. [13] found that the viscosity of the CaO–Al_2O_3 based mold flux rapidly decreased at first and then gradually stabilized stable with C/A ratio changes above 1270 °C. Kim and Park [14] revealed that the slag viscosity decreased with increasing C/A ratio, which was due to the decrease in the degree of polymerization. These cases mainly focus on the mold flux containing SiO_2; however, little information is available on the effect of the C/A ratio on the aluminate structure only. Additionally, although several studies [15–19] have been conducted on the structural relationship of mold flux containing a large amount of alkali metal oxides or B_2O_3, the higher electroslag smelting temperature has caused more significant volatilization. Alternative oxides should be added as little as possible.

Therefore, the effect of the CaF_2 and C/A ratio on the viscosity and structure of the ESR CaF_2–CaO–Al_2O_3–MgO–TiO_2 slag system in the present work was evaluated using the rotating cylinder method, Fourier transform infrared (FTIR) spectroscope, and Raman spectroscope. Furthermore, the activity coefficient is introduced to explain the phenomenon of change in the viscosity and structural units from a thermodynamic point of view.

2 Experimental

2.1 Sample preparation

Reagent-grade powders of CaF_2, CaO, Al_2O_3, MgO, and TiO_2 were prepared to produce slag samples. To remove moisture and impurities, CaO, Al_2O_3, and MgO powders were calcined at 1000 °C, and CaF_2 and TiO_2 powders were heated to 500 °C for 4 h in a muffle furnace before being synthesized. All samples were mixed in a mortar for 30 min to obtain a well-proportioned composition of the slag samples, which were then pre-melted in a platinum crucible protected by a corundum crucible in a high-temperature furnace at 1500 °C for 5 min to ensure homogenous chemical composition. The molten slag was rapidly quenched in cold water, followed by drying at 120 °C for 4 h in a bake oven, crushed, and ground into fine particle powders which were used to detect the slag structure. The chemical composition was determined by chemical analysis, where the F^- concentration was measured using the ion selective electrode method. The chemical compositions of the slag before and after pre-melting are listed in Tables 1 and 2, respectively.

2.2 Viscosity measurement

The rotating cylinder method was employed to determine the viscosity of the synthesized slags using an HRV-1600P viscometer (Sinosteel Luoyang Institute of Refractories Research Co., Ltd., Luoyang, China). A schematic diagram of the experimental apparatus and the dimensions of the graphite crucible are presented in Fig. 1 and Table 3, respectively. To achieve accurate and effective viscosity values, calibration measurements were carried out at room temperature using the known viscosity of standard castor oil in a constant-temperature water bath. A graphite crucible containing 300 g of weighed slag was placed in a high-temperature pit furnace with high-load U-type $MoSi_2$ electric bars at a heating rate of 10 °C/min and heated from room temperature to the target temperature of 1470, 1520, 1570, and 1620 °C; and this temperature was maintained for 30 min. The furnace body was then raised so that the Mo spindle was immersed in the molten slag and rotated at approximately 30 r/min. A computer was used to record automatically and calculate the average to obtain a precise viscosity value at the target temperature point. During the entire viscosity measurement, both the graphite crucible and spindle were properly aligned along the axis of the viscometer to avoid light deviations, and argon gas (99.99%) was used as a protective atmosphere with a flow rate of 50 mL/min.

Table 1 Chemical composition of slag samples before pre-melting

Sample	Chemical composition/wt.%					C/A ratio
	CaF_2	CaO	Al_2O_3	MgO	TiO_2	
C1	15.0	37.5	37.5	2.0	8.0	1.0
C2	20.0	35.0	35.0	2.0	8.0	1.0
C3	25.0	32.5	32.5	2.0	8.0	1.0
C4	30.0	30.0	30.0	2.0	8.0	1.0
C5	25.0	28.9	36.1	2.0	8.0	0.8
C6	25.0	35.5	29.5	2.0	8.0	1.2
C7	25.0	37.9	27.1	2.0	8.0	1.4

Table 2 Chemical composition of slag samples after pre-melting

Sample	Chemical composition/wt.%					C/A ratio
	CaF_2	CaO	Al_2O_3	MgO	TiO_2	
C1	14.1	39.7	36.1	2.1	8.0	1.1
C2	19.2	36.7	33.7	2.4	8.0	1.1
C3	23.8	34.7	31.0	2.3	8.3	1.1
C4	28.6	32.5	28.7	2.1	8.2	1.1
C5	23.7	31.9	34.3	1.9	8.2	0.9
C6	23.6	37.0	28.9	2.2	8.3	1.3
C7	23.4	39.9	26.1	2.3	8.4	1.5

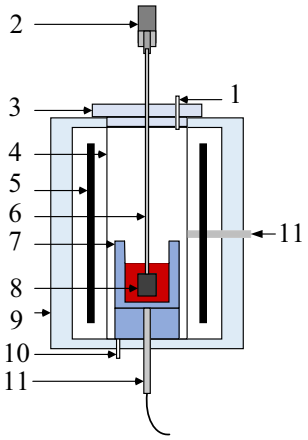

Fig. 1 Schematic diagram of experimental apparatus. 1—Gas outlet; 2—viscometer; 3—firebrick lid; 4—alumina tube; 5—$MoSi_2$ heating element; 6—shaft; 7—graphite crucible; 8—Mo spindle; 9—refractory; 10—gas inlet; 11—B-type thermocouple

Table 3 Dimensions of graphite crucible and spindle (mm)

Graphite crucible	Size	Mo spindle	Size
Inner diameter	50	Diameter	15
Outer diameter	60	Height	20
Height	80	Submerged length	20

2.3 FTIR and Raman spectra measurement

The quenched slag was measured using a Fourier transform infrared spectroscope (Nicolet, Summit, USA) and a laser confocal Raman spectrometer (Nicolet, Dxr 2Xi, USA) to determine the slag structure. FTIR spectra were recorded in the wave number range of 400–4000 cm^{-1} at room temperature and equipped with a KBr detector with a spectral resolution of 4 cm^{-1} and a scan number of 32. The sample for infrared measurement consisted of 2.0 mg slag and 200 mg KBr, which were mixed thoroughly in an agate mortar, and then pressed into a disk with a diameter of 13 mm. The Raman spectra of the samples were collected at room temperature in the frequency range of 200–1500 cm^{-1} using a laser confocal Raman spectrometer with an excitation wavelength of 532 nm. The Raman spectra were fitted by assuming Gaussian functions for the peaks of various structural units using Peak Fit V4 Software.

3 Results and discussion

3.1 Effect of CaF_2 and C/A ratio on slag viscosity

The viscosities of the CaF_2–CaO–Al_2O_3–MgO–TiO_2 slag with different CaF_2 contents and C/A ratios are shown in Fig. 2a, b, respectively. It can be observed that as the CaF_2 content gradually increases, the slag viscosity decreases correspondingly. This result is consistent with that of several studies [20, 21]. Meanwhile, the higher the temperature, the lower the viscosity. At a high temperature of 1620 °C, the addition of CaF_2 to slag had a slight effect on the viscosity from 0.089, 0.074, 0.064, to 0.057 Pa s with CaF_2 contents of 14.1, 19.2, 23.8 and 28.6 wt.%.

CaF_2 plays a significant role in the viscosity of the ESR slag. There are three ways to reduce the viscosity of slag by CaF_2. First, CaF_2 acts as a diluter in the slag and does not affect the relative distribution of the Q^i units [22]. Second, the complex structural units are depolymerized owing to the reduced degree of polymerization [9, 14, 23, 24]. Third, the addition of CaF_2 causes part of the non-bridging oxygen in the structure to be replaced by F^- ions, which leads to structural relaxation [20]. The influence of CaF_2 on the slag structure is complicated, which is similar to the findings in Refs. [21, 25]. Hence, it is essential to evaluate the role of CaF_2 in the slag structure.

In the experimental temperature range from 1470 to 1620 °C, the slag viscosity exhibits a downward trend with an increase in the C/A ratio or temperature, similar to the above-mentioned influence of CaF_2 on viscosity. In terms of the influence of oxides in the slag structure, CaO acts as a network modifier; Al_2O_3 is an amphoteric oxide and its amphoteric behavior on the structure is complicated. Furthermore, another new amphoteric oxide, TiO_2, was introduced into the slag, resulting in a pronounced change in the preceding aluminate structure [12].

3.2 Effect of CaF_2 and C/A ratio on apparent activation energy for viscous flow

The apparent activation energy of viscous flow is regarded as the minimum energy required to overcome the resistance between fluids; that is, the more complicated the network

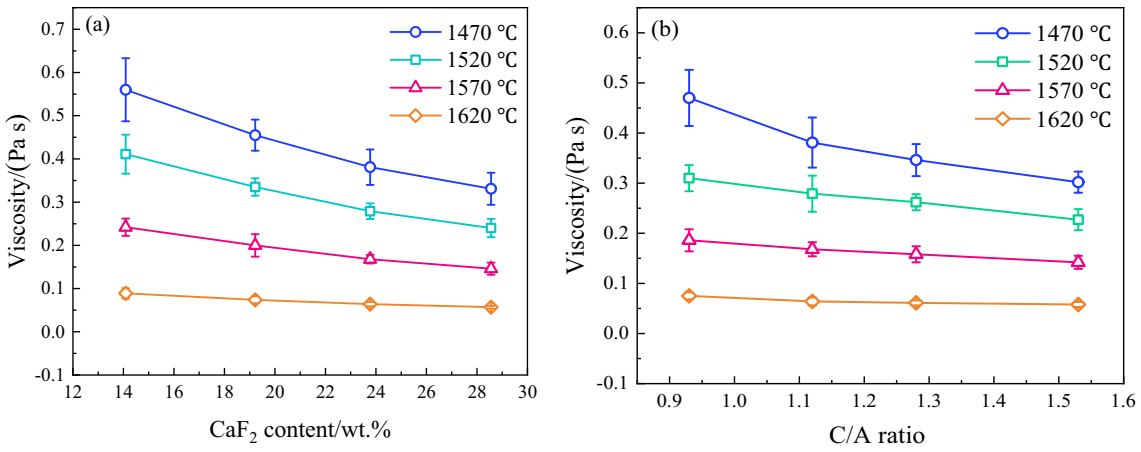

Fig. 2 Viscosities of CaF_2–CaO–Al_2O_3–MgO–TiO_2 slag with different CaF_2 contents (**a**) and C/A ratios (**b**)

structure, the higher the apparent activation energy of the viscous flow [26]. Therefore, the apparent activation energy can be used to clarify the relationship between slag viscosity and the corresponding structure. Generally, apparent activation energy for viscous flow is calculated in terms of the Arrhenius-type equation as follows:

$$\eta = A\ \exp(E_\eta/(RT)) \tag{1}$$

where η is the viscosity, Pa s; A is the pre-exponential factor, Pa s; E_η is the apparent activation energy for viscous flow, J/mol; R is the ideal gas constant, J/(mol K); and T is the absolute temperature, K.

The natural logarithm of the viscosity and reciprocal of temperature multiplied by R is fitted based on the experimental results of four temperature points of each slag, and the correlation coefficient is in the range of 0.882–0.934. It indicates that the linear fitting is not good enough and follows the Newtonian fluid poorly. However, it can be found that the natural logarithm of the viscosity and reciprocal of temperature multiplied by R has a better linear fitting with the correction coefficient from 0.973 to 0.989 at the three temperature points of 1470, 1520, and 1570 °C of each slag. Therefore, linear fitting calculation is carried out using the viscosity value of three temperature points. Based on Eq. (1), the natural logarithm of the viscosity and reciprocal of temperature multiplied by R can be obtained, as shown in Fig. 3a, b, corresponding to the effect of the CaF_2 and C/A ratio on the apparent activation energy for viscous flow, respectively. The apparent activation energy for viscous flow can be calculated from the slope of the natural logarithm of viscosity versus the reciprocal of the temperature multiplied by R.

The apparent activation energy for the viscous flow of the CaF_2–CaO–Al_2O_3–MgO–TiO_2 slag system with varying CaF_2 contents and C/A ratios is shown in Fig. 4a, b. The apparent activation energy was first significantly reduced and then slightly decreased with increasing CaF_2 content. However, increasing the C/A ratio notably decreased the apparent activation energy for viscous flow. These results indicate that both the CaF_2 and C/A ratio can affect the structure of the slag; however, the effect of the C/A ratio on the structure is higher than that of CaF_2, according to the variation of the CaF_2 and C/A ratio affecting the apparent activation energy for viscous flow in the research range. Moreover, the relative resistance of the fluid at high temperatures decreases, which also explains the change in the apparent activation energy of the corresponding slag.

3.3 Effect of CaF_2 and C/A ratio on slag structure using FTIR

The FTIR spectra of the CaF_2–CaO–Al_2O_3–MgO–TiO_2 slag system are shown in Fig. 5a, b as a function of the wave number with different CaF_2 contents and C/A ratios, respectively. The typical spectra of calcium aluminate slag can be divided into three bands: 720–940 cm^{-1}, 600–720 cm^{-1}, and 500–600 cm^{-1}, corresponding to the asymmetric stretching vibration of the [AlO_nF_{4-n}]-tetrahedral complexes (n = 0–4), [AlO_4]-tetrahedra, and [AlO_6]-octahedra, respectively [27].

The asymmetric stretching vibration of the [AlO_nF_{4-n}]-tetrahedral complexes with various CaF_2 contents remained unchanged, indicating no depolymerization of the complex structure. The transmitting bands of the [AlO_nF_{4-n}]-tetrahedral complexes appear in the fluoroaluminate system based on a study by Park et al. [27]. In the basic slag calcium fluoride, they are mainly present as F^- and Ca^{2+} ions according to Tsunawaki et al. [28], who illustrated that a small amount of F^- ions exist in [AlO_nF_{4-n}]-tetrahedral complexes and most of the fluorides are present as F^- ions in the CaF_2–CaO–Al_2O_3–MgO–TiO_2 slag system. The

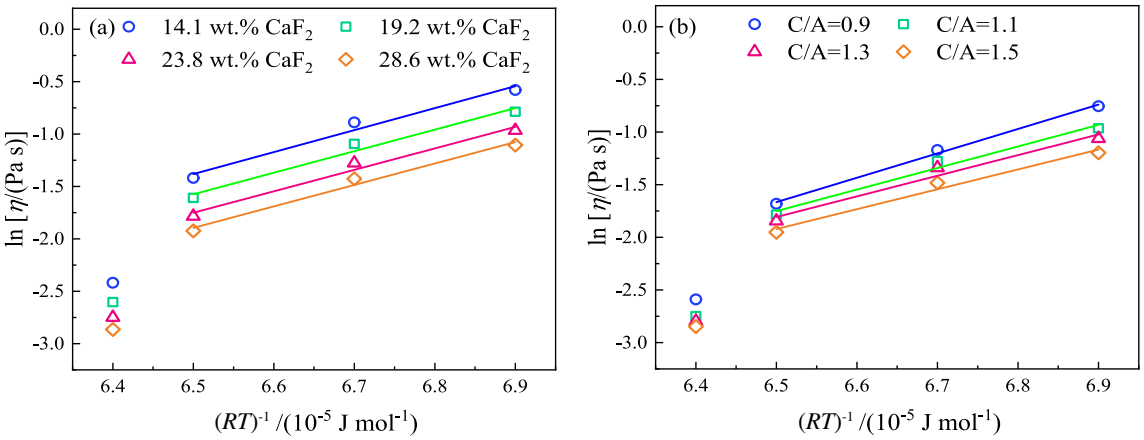

Fig. 3 Temperature dependence for viscous flow of CaF_2–CaO–Al_2O_3–MgO–TiO_2 slag with varying CaF_2 contents (**a**) and C/A ratios (**b**)

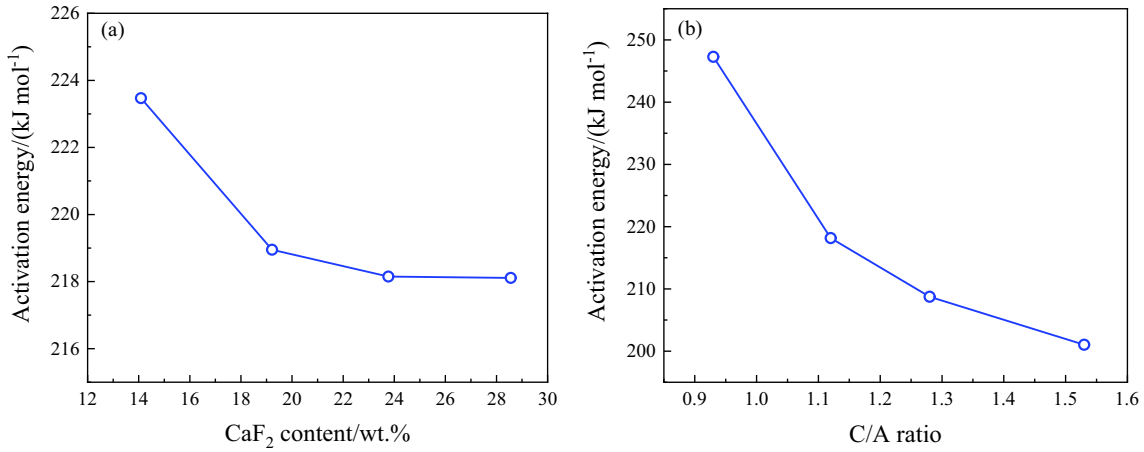

Fig. 4 Apparent activation energy for viscous flow of slag samples with varying CaF_2 contents (**a**) and C/A ratios (**b**)

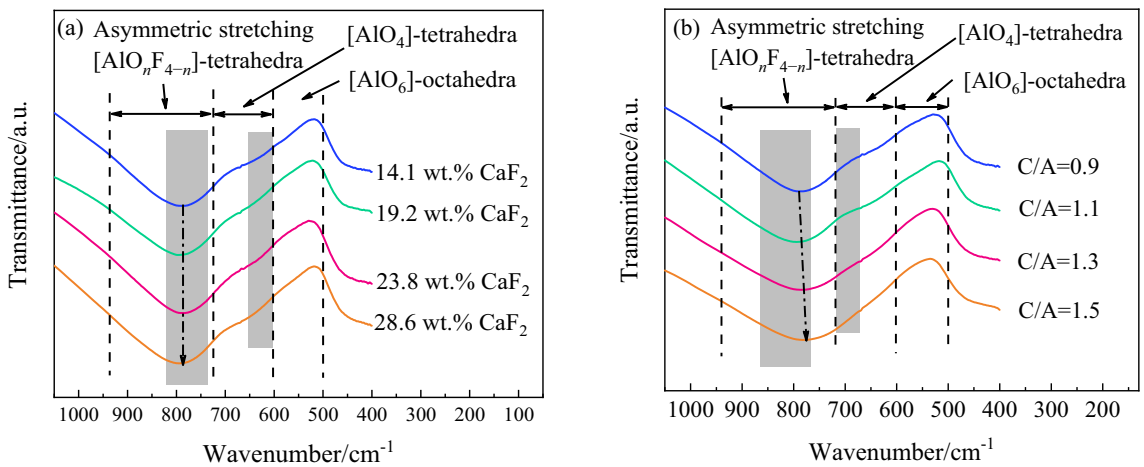

Fig. 5 FTIR spectra of CaF_2–CaO–Al_2O_3–MgO–TiO_2 slag with varying CaF_2 contents (**a**) and C/A ratios (**b**)

characteristic Al–O stretching vibration in the $[AlO_4]$-tetrahedra occurs at a wave number of approximately 660 cm^{-1} within the range of 600–720 cm^{-1}, and there is a slight effect on the structure with different CaF_2 contents. Simultaneously, $[AlO_6]$-octahedra with a wave number range of 500–600 cm^{-1} is not found. These results indicate

that CaF_2 mainly exists as Ca^{2+} ions and F^- ions in the slag structure, accompanied by slight depolymerization of the structure.

For the effect of the C/A ratio on the slag structure, it was found that the center of gravity of the $[AlO_nF_{4-n}]$-tetrahedral complexes shifted from approximately 793–780 cm^{-1} with increasing C/A ratio, indicating that the $[AlO_nF_{4-n}]$-tetrahedral complexes were destroyed. Additionally, the stretching vibrations of the Al–O bond in the $[AlO_4]$-tetrahedra at 660 cm^{-1} have a gentle slope and accumulate with an increase in the C/A ratio, indicating a slight change in the $[AlO_4]$-tetrahedra. Similarly, $[AlO_6]$-octahedra did not appear.

For the structural properties of the slag, FTIR spectroscopy is complementary to Raman spectroscopy; for example, FTIR spectroscopy is highly sensitive to polar groups, whereas non-groups are sensitive. Moreover, the Raman spectra can be identified for further quantitative analysis of the structural units.

3.4 Effect of CaF_2 and C/A ratio on slag structure using Raman spectra

At room temperature, the original Raman spectra for the CaF_2–CaO–Al_2O_3–MgO–TiO_2 slag system with varying CaF_2 contents and C/A ratios are illustrated in Fig. 6a, b, respectively. It can be observed that the original Raman spectra for different CaF_2 contents have a similar curve type, which indicates that CaF_2 has no effect on the slag structure. In contrast to the original Raman spectra, the peak near 550 cm^{-1} gradually deceases and the Raman peak moves toward a lower frequency from 804 to 792 cm^{-1} with an increase in the C/A ratio. These results indicate that increasing the C/A ratio depolymerizes the aluminate structure. The structural changes caused by CaF_2 and the C/A ratio in the Raman spectra are consistent with the FTIR spectra.

Based on the Gaussian deconvolution method, the Raman spectra were deconvoluted with a minimum correction coefficient above 0.997 and all the backgrounds of the Raman signals were subtracted before fitting. According to the Raman spectrum corresponding to the aluminate structure, the selected wave number range was from 490 to 950 cm^{-1}. From the deconvolution of Fig. 7a–g, the characteristic peak of the Al–O–Al linkage is approximately 550 cm^{-1}, which is due to the transverse motions of bridging oxygens in the $[AlO_4]$-tetrahedral network structure [29, 30]. The band near 756 cm^{-1} corresponds to the Al–O stretching vibration in the $[AlO_4]$-tetrahedral units with two bridging oxygens, assigned as Q^2 (non-bridging oxygen per tetrahedrally coordinated cation, NBO/Al = 2), and the band at approximately 790 cm^{-1} is seized by four bridging oxygens, deemed as Q^4 (NBO/Al = 0), according to previous studies [29, 31]. Moreover, for the slag containing TiO_2, the Raman spectra in the wave number range of 700–728 and 820–843 cm^{-1} can be considered as the appearance of new bands, corresponding to the O–Ti–O deformation vibration and $Ti_2O_6^{4-}$ chains in the slag structure, respectively [32]. The distributions of all the structural units are listed in Table 4.

The variation in the relative fraction of each bond in the Raman structural units and relative height of the Al–O–Al linkage are presented in Fig. 8a, b with different CaF_2 contents and C/A ratios, respectively. It can be concluded that with an increase in the CaF_2 content, all structural units remained basically unchanged, but when the CaF_2 content was 28.6 wt.%, there were subtle changes; for example, Q^2 increases and the Al–O–Al linkage decreases slightly. This phenomenon shows that CaF_2 added to slag has a slight influence on the structure because of the trace production of Al–F bonds through the FTIR analysis of the $[AlO_nF_{4-n}]$-tetrahedral complexes [27], and previous studies have shown that the Raman bands near 530 cm^{-1}

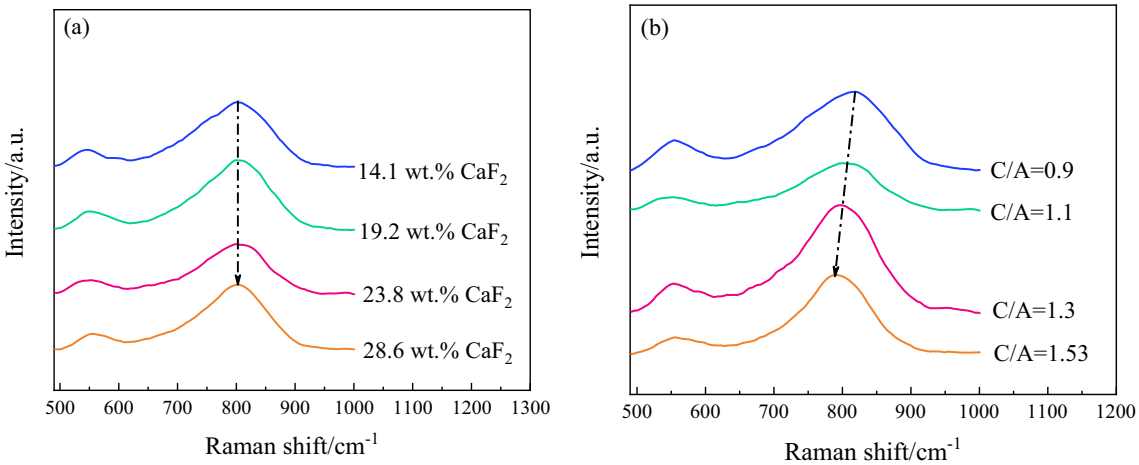

Fig. 6 Original Raman spectra for CaF_2–CaO–Al_2O_3–MgO–TiO_2 slag with varying CaF_2 contents (**a**) and C/A ratios (**b**)

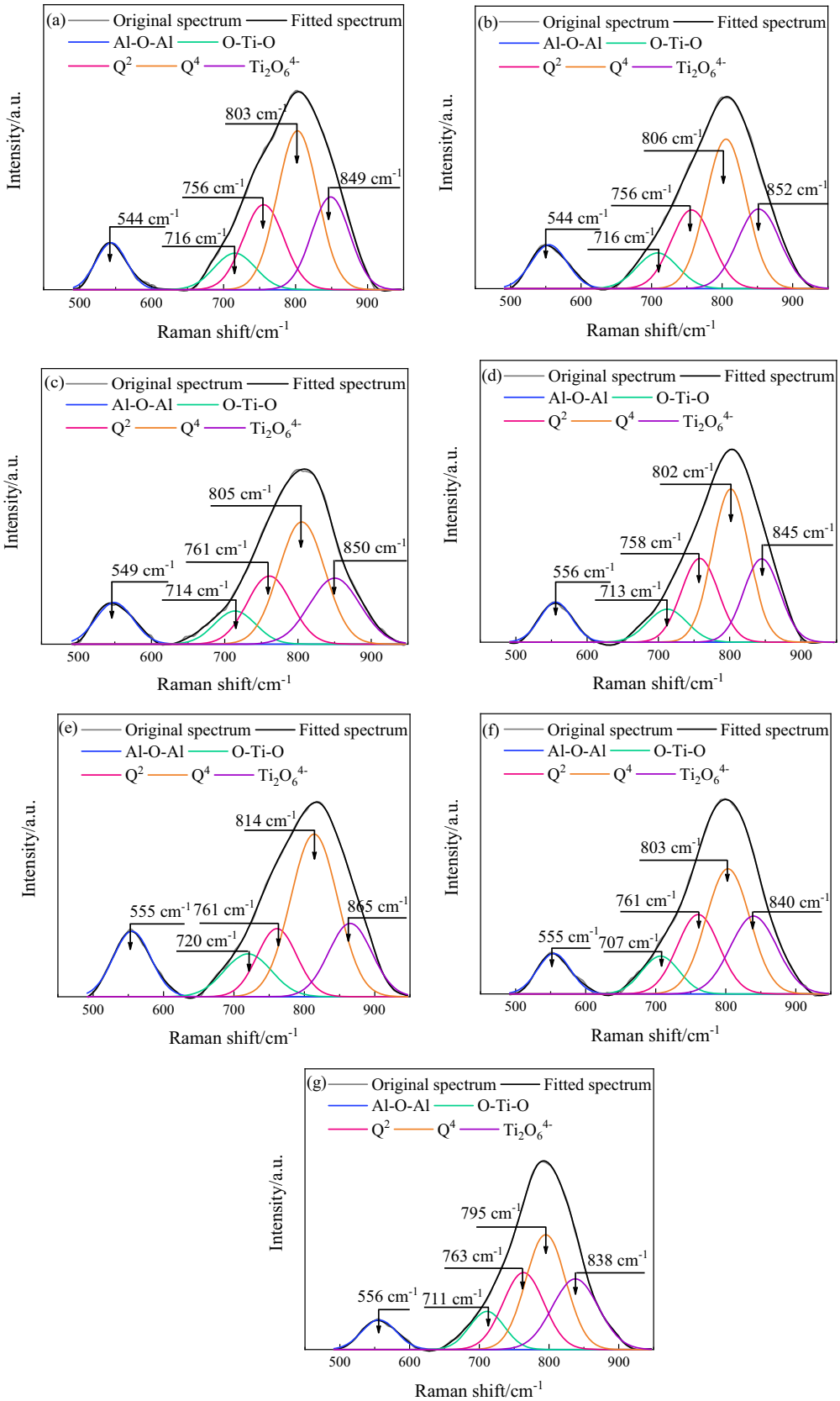

Fig. 7 Typical deconvoluted peaks of Raman spectra from slags. **a** Slag C1; **b** slag C2; **c** slag C3; **d** slag C4; **e** slag C5; **f** slag C6; **g** slag C7

Table 4 Distribution of all structural units

Structural unit	Wave number/cm^{-1}	Ref.
Al–O–Al linkage	550	[29, 30]
Q^2 unit in [AlO_4]	756	[31]
Q^4 unit in [AlO_4]	790	[29, 31]
O–Ti–O deformation vibration	700–728	[32]
$Ti_2O_6^{4-}$ chains	820–843	[32]

correspond to Al–F stretching vibration in AlF_6 octahedral units [27, 33]. According to Lee and Min [20], the change in the apparent activation energy for viscous flow is closely related to the relaxation effect of the anionic species by the formation of NBO–Ca^{2+}–F^- and the hindrance effect of the cationic species by the formation of NBO–Ca^{2+}–NBO, except for the depolymerization effect. Therefore, it can be concluded that CaF_2 mainly exists in the slag structure in the form of NBO–Ca^{2+}–F^- and NBO–Ca^{2+}–NBO, and its content increases with increasing CaF_2 content, which is due to the decrease in the apparent activation energy for viscous flow.

As the C/A ratio increased, the relative height of the Al–O–Al linkage gradually decreased, which indicated that the slag aluminate structure was depolymerized. In the [AlO_4]-tetrahedral network structure, the Q^4 units decrease and the Q^2 units increase because the Q^4 units are depolymerized into Q^2 units [34]. Furthermore, the relative fraction of $Ti_2O_6^{4-}$ chains increases and that of O–Ti–O chains decreases as the C/A ratio increases, resulting in the formation of relatively simple structural units. Consequently, the degree of depolymerization of the aluminate network structure decreases with increasing the C/A ratio, which is consistent with the change in viscosity.

Through FTIR and Raman analysis, CaF_2, mainly in terms of the relaxation effect, affects the slag structure, whereas the C/A ratio affects the slag structure through the depolymerization effect. It can be concluded that the C/A ratio has a greater impact on the slag structure than the CaF_2 content, which is in accordance with the comparison of the corresponding viscosity values at the same temperature point.

3.5 Thermodynamic activity coefficients and slag structure

Through the above analysis, the CaF_2 and C/A ratios decreased the viscosity and affected the slag structure in the aluminate structure. Based on the thermodynamic analysis of the molten slag, the activity coefficient is introduced to analyze the viscosity and structure. Previous studies by Park et al. [35] and Chen et al. [19] have reported that the macroscopic thermophysical phenomena of molten slags could originate from changes in the microscopic structure. Taking pure solid as the standard state, the activity values were calculated using the oxide database FToxid in the thermodynamic software FactSage 7.1. The parameters of γ_i can be calculated using the following equation:

$$\gamma_i = \frac{a_i}{x_i} \tag{2}$$

where γ_i, a_i, and x_i are the activity coefficient, activity, and mole fraction of the component i, respectively.

The activity coefficients of CaF_2 and C/A ratio in the slag are shown in Fig. 9a, b as a function of CaF_2 and C/A ratio, respectively, where the activity coefficient of the C/A ratio is the ratio of the activity coefficients of CaO and Al_2O_3. $\gamma_{CaF_2,C/A}$ represents the change in the activity

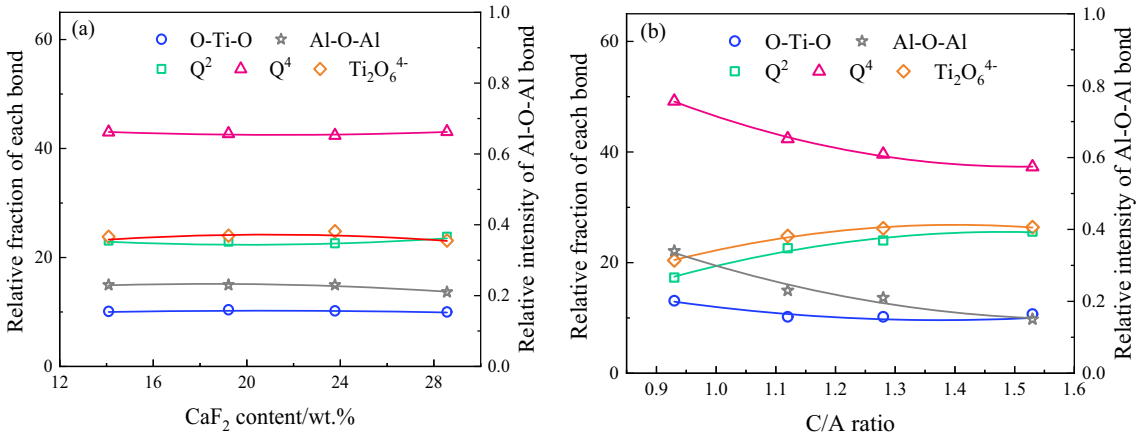

Fig. 8 Relative fraction of each bond and relation height of Al–O–Al bond for CaF_2–CaO–Al_2O_3–MgO–TiO_2 slag with different CaF_2 contents (**a**) and C/A ratios (**b**)

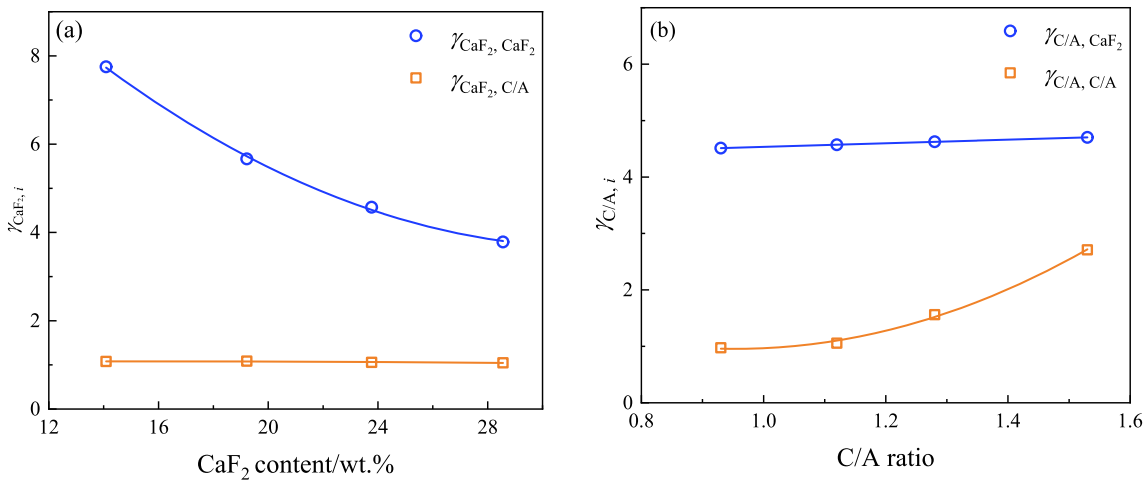

Fig. 9 Activity coefficients of CaF_2 and C/A ratio with varying CaF_2 contents (**a**) and C/A ratios (**b**)

coefficient of the C/A ratio with various CaF_2 contents; γ_{CaF_2,CaF_2} represents the change in the activity coefficient of CaF_2 with various CaF_2 contents; $\gamma_{C/A,CaF_2}$ represents the change in the activity coefficient of CaF_2 with various C/A ratios; and $\gamma_{C/A,C/A}$ represents the change in the activity coefficient of the C/A ratio with various C/A ratios. With an increase in the CaF_2 content, the activity coefficients of CaF_2 and the C/A ratio were positively correlated and that of CaF_2 decreased gradually, whereas that of the C/A ratio changed slightly. It can be suggested that CaF_2 is in the form of NBO–Ca^{2+}–NBO, and NBO–Ca^{2+}–F^- bonds stably exist in the slag through structural analysis, which causes a decrease in the bonding strength of the aluminate structure; thus, it has a trifling effect on the aluminate structure. Additionally, more O^{2-} and Ca^{2+} ions appear with increasing C/A ratio, resulting in the intensification of the depolymerization of the aluminate structure. Consequently, the activity coefficient of the C/A ratio increased. Simultaneously, the activity coefficient of CaF_2 is increased slightly, which may be because a small amount of CaO destroyed the bond with F^- ions by the substitution of the bridging oxygen, thereby releasing a few Ca–F bonds.

It can be inferred that with the change in CaF_2 and the C/A ratio, the activity coefficient of the same species has a pronounced impact on each other, whereas the effect of different species is not significant. Therefore, a relatively stable CaF_2 content and C/A ratio were obtained through the comparison of Fig. 9a, b from the perspective of thermodynamics, that is, the CaF_2 is 23.0 wt.%, and the C/A ratio is 1.1.

4 Conclusions

1. The slag viscosity decreases with an increase in the CaF_2 and CaO/Al_2O_3 ratio, and the apparent activation energy for the viscous flow of CaF_2–CaO–Al_2O_3–MgO–TiO_2 slag also decreases.
2. The increase in the CaF_2 concentration does not affect the [AlO_4]-tetrahedral structural units; however, it is closely related to the relaxation effect of the formation of NBO–Ca^{2+}–F^- and the hindrance effect of the cationic species by the formation of NBO–Ca^{2+}–NBO.
3. Increasing the CaO/Al_2O_3 ratio leads to the depolymerization of some Q^4 units in the [AlO_4]-tetrahedra structure into Q^2 units, whereas the relative fraction of $Ti_2O_6^{4-}$ chains increases and that of O–Ti–O chains decreases.
4. The CaO/Al_2O_3 ratio had a greater impact on the slag structure than the CaF_2 content. Based on the thermodynamic analysis, the variation in the activity coefficients of CaF_2 and the CaO/Al_2O_3 ratio can indirectly explain the relationship between viscosity and structure in the slag.

Acknowledgements This study was funded by the National Natural Science Foundation of China (No. 51774225).

References

[1] B.E. Paton, L.B. Medovar, Steel Transl. 38 (2008) 1028–1032.
[2] C.B. Shi, Y. Huang, J.X. Zhang, J. Li, X. Zheng, Int. J. Miner. Metall. Mater. 28 (2021) 18–29.

[3] C.B. Shi, J. Li, J.W. Cho, F. Jiang, I.H. Jung, Metall. Mater. Trans. B 46 (2015) 2110–2120.
[4] M. Schwenk, B. Friedrich, Role and effects of slag components in ESR processes, ALD Workshop, Hanau, Germany, 2016.
[5] C.B. Shi, ISIJ Int. 60 (2020) 1083–1096.
[6] C.B. Shi, S.H. Shin, D.L. Zheng, J.W. Cho, J. Li, Metall. Mater. Trans. B 47 (2016) 3343–3349.
[7] J.T. Ju, G.H. Ji, J.L. An, C.M. Tang, Ironmak. Steelmak. 48 (2021) 109–115.
[8] Y.G. Lao, Y.M. Gao, F.J. Deng, Q. Wang, G.Q. Li, Metall. Res. Technol. 116 (2019) 638.
[9] J.H. Park, D.J. Min, H.S. Song, ISIJ Int. 42 (2002) 344–351.
[10] A. Mitchell, Can. Metall. Quart. 20 (1981) 101–112.
[11] J.T. Ju, G.H. Ji, C.M. Tang, J.L. An, Steel Res. Int. 91 (2020) 2000111.
[12] J.T. Ju, K.S. Yang, G.H. Ji, Z.H. Zhu, S.W. Liu, Rare Metal Mater. Eng. 49 (2020) 3676–3682.
[13] W. Yan, W. Chen, Y. Yang, C. Lippold, A. McLean, Ironmak. Steelmak. 42 (2015) 698–704.
[14] T.S. Kim, J.H. Park, ISIJ Int. 54 (2014) 2031–2038.
[15] J.L. Li, K.C. Chou, Q.F. Shu, ISIJ Int. 60 (2020) 51–57.
[16] L. Zhang, B.Y. Zhai, W.L. Wang, I. Sohn, J. Sustain. Metall. 7 (2021) 559–568.
[17] H.Q. Shao, E.Z. Gao, W.L. Wang, L. Zhang, J. Am. Ceram. Soc. 102 (2019) 4440–4449.
[18] Y. Hou, G.H. Zhang, K.C. Chou, J. Alloy. Compd. 856 (2021) 158239.
[19] Z.W. Chen, H. Wang, Y.Q. Sun, L.L. Liu, X.D. Wang, Metall. Mater. Trans B 50 (2019) 2930–2941.
[20] S. Lee, D.J. Min, J. Am. Ceram. Soc. 100 (2017) 2543–2552.
[21] G.H. Zhang, K.C. Chou, Ironmak. Steelmak. 40 (2013) 376–380.
[22] Y. Sasaki, M. Iguchi, M. Hino, ISIJ Int. 47 (2007) 346–347.
[23] R.W. Luth, Am. Miner. 73 (1988) 297–305.
[24] Q. Gao, Y. Min, C.J. Liu, M.F. Jiang, J. Iron Steel Res. Int. 24 (2017) 1152–1158.
[25] Q.F. Shu, Z. Wang, K.C. Chou, Steel Res. Int. 82 (2011) 779–785.
[26] S.C. Gao, K.X. Jiao, J.L. Zhang, Philo. Mag. 99 (2019) 853–868.
[27] J.H. Park, D.J. Min, H.S. Song, ISIJ Int. 42 (2002) 38–43.
[28] Y. Tsunawaki, N. Iwamoto, T. Hattori, A. Mitsuishi, J. Non-Cryst. Solids 44 (1981) 369–378.
[29] P. McMillan, B. Piriou, J. Non-Cryst. Solids 55 (1983) 221–242.
[30] B.O. Mysen, M.J. Toplis, Am. Miner. 92 (2007) 933–946.
[31] M. Licheron, V. Montouillout, F. Millot, D.R. Neuville, J. Non-Cryst. Solids 357 (2011) 2796–2801.
[32] B.O. Mysen, F.J. Ryerson, D. Virgo, Am. Miner. 65 (1980) 1150–1165.
[33] J. Yang, J.Q. Zhang, O. Ostrovski, C. Zhang, D.X. Cai, Metall. Mater. Trans. B 50 (2019) 1766–1772.
[34] B. Mysen, D. Neuville, Geochim. Cosmochim. Acta 59 (1995) 325–342.
[35] J.H. Park, D.S. Kim, Y.D. Lee, H.S. Song, D.J. Min, in: VII International Conference on Molten Fluxes and Salts, The South African Institute of Mining and Metallurgy, Cape Town, South African, 2004, pp. 157–164.